ACS OMEGA

http://pubs.acs.org/journal/acsodf

Article

Effect of the Standardized ZnO/ZnO-GO Filter Element Substrate driven Advanced Oxidation Process on Textile Industry Effluent Stream: Detailed Analysis of Photocatalytic Degradation Kinetics

Kirtiman Singh, Shiwangi Maurya, Surabhi Gupta, Nihar Ranjan, Gurunath Ramanathan, and Shantanu Bhattacharya*

Cite This: *ACS Omega* 2023, 8, 28615−28627

Read Online

ACCESS | Metrics & More | Article Recommendations | Supporting Information

ABSTRACT: A simple process of synthesizing coated filter element substrates (FES) containing zinc oxide (ZnO) nanorods and ZnO graphene-oxide nanocomposite for a pilot-scale industrial dye-effluent treatment plant is proposed. This work reports a detailed analysis of the photocatalysis mechanism on real industrial effluent streams containing a mixture of dyes. The analysis is very relevant for conducting advanced oxidation process-assisted effluent remediation at a field-level treatment operation. Estimation of the dye concentration shows nearly complete (≥98%) degradation from an initial dye sample concentration. A detailed study for the analysis of the initial reactive dyes and their degradation products was performed for quantification and identification of the degradation products through various spectral techniques. A design of the remediation mechanism through degradation pathways is proposed for characterizing the organic compounds in the degraded dye products. A regeneration and reusability study was performed on the FES presenting the durability of the FES-designed synthesis process originally for 11 cycles and regenerated FES for six cycles for achieving a threshold of 60% degradation efficiency. The experimental results demonstrate the efficacy of FES through the designed immobilized approach for the complete remediation of textile dye effluents for a 4 h treatment plant process and the consistent operability of the FES for the combined dye wastewater treatment operations.

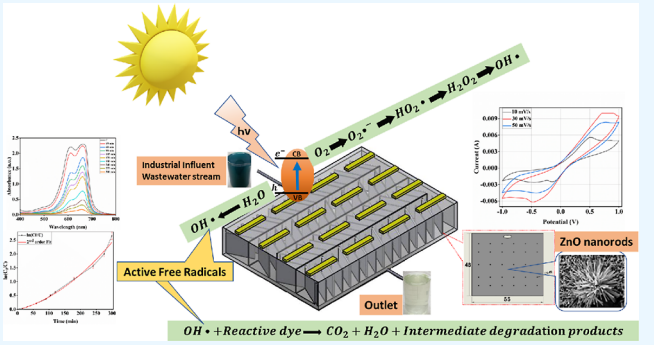

1. INTRODUCTION

Remediation of the industrial pollutants which are discharged into the environment presents increasing challenges to sustainable design goals. The reactive dyes used in textile industries are often difficult to remove due to their composite molecular structures,[1] high color pigmentation, high water solubility, and toxicity. The inability to remove textile dyes from wastewater greatly impacts natural water bodies when discharged with partial treatment.[2−4] As a result, treatment of such discharges from industrial effluents is essential to prevent the vulnerability of the affected ecosystem.

Remediation of industrial effluent wastewater is carried out in several ways with sedimentation being a prevalent means of separation for heterogeneous systems where the heavy components can be separated easily.[5] In liquid systems where the pollutant is miscible, this separation becomes challenging.[6] Dye remediation is often achieved using techniques such as chemical treatment,[7] biological treatment,[8] physio-chemical and biochemical treatment,[9] membrane-separation technologies,[10] nanotechnology-based interventions,[11] and adsorption processes.[12] Of these, advanced oxidation process (AOP)-based wastewater treatment techniques are gaining significant attention.[13] The catalysts prominently used in AOP processes are modified to enhance the degradation efficiency through morphological changes, functionalization, and band gap engineering.[14,15]

Various AOP-based metal-oxide semiconductor catalysts are known in the literature for remediation of dyes such as iron oxide (Fe_2O_3; 2.2 eV),[16] vanadium oxide (V_2O_5; 2.8 eV),[17,18] zinc oxide (ZnO; 3.2 eV),[19,20] titanium oxide (TiO_2; 3.2 eV),[21] etc. Among these, the ZnO-based catalyst systems are known for having robust catalytic properties, low cost and simple fabrication process, small band gap, and nontoxic nature.[22] ZnO-based nanostructures such as nanowires,[23,24] nanorods,[25] nanoflowers, and so forth are already established in the literature for methylene blue (MB) dye degradation.[26]

Received: May 6, 2023
Accepted: July 14, 2023
Published: July 24, 2023

https://doi.org/10.1021/acsomega.3c03122
ACS Omega 2023, 8, 28615−28627

However, these materials have some drawbacks of slightly higher function and lower light absorption capacity which can be addressed through the synthesis of new "filter element substrates (FES)". The nanomaterial composites have complementary additive surface properties, leading to better performance in dye removal systems than the constituents' material themselves. The synthesized nanocomposite finds its usefulness through significant improvement by lowering the work function and modulation of the recombination rates of the photoexcited pairs through the process of hybridization.[27]

Metal oxide-based semiconductors having catalytic properties and their nanocomposites are well-known in the literature for dye remediation applications.[28−31] Research in our laboratory has also highlighted the use of such metal oxide-based nanocomposites in different remediation contexts showing their importance in the development of next-generation remediation agents.[19,20,32] Authors have previously published the use of ZnO/GO nanoflowers for improved decolorization of MB dye.[33] However, this nanocomposite has certain limitations for the treatment process such as inadequate immobilized retention to the FES and the complex synthesis process of the nanocomposite. To overcome these limitations, we report herein the use of an easily synthesized and more efficient ZnO/zinc oxide graphene oxide (ZnO-GO) nanocomposite as a new FES for the remediation of real textile effluent streams.

In this article, a simple, cost-effective, and efficient facile synthesis of ZnO and ZnO-GO nanocomposites for the fabrication of a "FES" using solution growth method is proposed. Using an array of analytical and microscopic techniques including high-performance liquid chromatography-mass spectrometry (HPLC)-(MS/MS), nuclear magnetic resonance (NMR), UV−vis, Fourier transform infrared spectroscopy (FTIR), field-emission scanning electron microscopy (FE-SEM), transmission electron microscopy (TEM), and so forth, the authors analyzed the design of the FES-based pilot plant. We have evaluated free-radical-induced fast reaction kinetics and the associated mechanism of the reaction processes for sunlight-induced remediation of the industrial dye in an aqueous medium. Subsequently, the identification of the degradation products for the industrial dye is achieved by mapping the pathways of degradation, and resultant degradation products are serially modeled based on the theoretical database analysis. The synthesized FES was further investigated for regeneration to ascertain the reusability of the photocatalyst using a photocatalytic pilot plant for an industrial-scale treatment process. We identified various intermediates of effluent industrial dyes in AOP-assisted degradation while correlating the possible mechanistic pathways.

2. MATERIALS AND METHODS

2.1. Materials and Chemicals. To fabricate the upstanding ZnO and ZnO-GO nanocomposite FES, the chemical agents for synthesis were purchased from commercial sources: zinc acetate [$Zn(Ac)_2$] of analytical grade, graphite powder pract. (100 μ), and potassium permanganate purified ($KMnO_4$) were purchased from S.D. Fine-chem Limited (99% purity) and used without any further modification. Methanol (CH_3OH) of analytical grade was purchased from Qualigens Fine Chemicals (99% purity). Sodium hydroxide pellets were purchased from Fischer Scientific (98% purity). Zinc nitrate hexahydrate $(Zn(NO_3)_2)\cdot 6H_2O$, hexamethylenetetramine (HMTA) (99% purity), hydrazine hydrate (80% AR), and sodium chloride (NaCl) (99.5% AR/ACS) were purchased from LOBA Chemicals Pvt Ltd. Sulfuric acid (H_2SO_4) (98% purity) and hydrochloric acid (HCl) (35% purity) were obtained from Merck Life Sciences Pvt. Ltd. Hydrogen peroxide (H_2O_2) of 30% (w/w) (98% purity) is obtained from Thermo Fischer Scientific India Pvt Ltd. All reagents were used as received. Deionized (DI) water was used in all the aqueous solutions and for all the laboratory experiments.

2.2. Dye Properties and Characterization. RB-4 dye (Procion blue MX-R, 1-Amino-4-[3-(4,6-dichlorotriazin-2-ylamino)-4-sulfophenylamino] anthraquinone-2-sulfonic acid) has been obtained from Sigma-Aldrich (3050 Spruce Street, Saint Louis, USA) and used without further modifications or purification. RB-4 (Empirical Formula: $C_{23}H_{14}Cl_2N_6O_8S_2$) consisting of 2-amino groups and a sulfonate group was used.[34] The commercial reactive dyes commonly used in textile industries are obtained from the Industrial Park, Jaipur for analysis. The C.I. reactive blue (CRB) is analyzed through NMR. The industrial dye-effluent samples are obtained from the wastewater treatment tank situated in Laxmi Textiles Pvt. Ltd., Textile Park, Jaipur, Rajasthan India. The samples are used without any further processing and filtered through a sieve net and 0.22 μm Durapore poly(vinylidene difluoride) (PVDF) membrane filter unit to discard the particle impurities.

2.3. Synthesis of Zinc-Oxide Nanorods (ZnO), Graphene-Oxide (GO), and Zinc-Oxide Graphene-Oxide Nanocomposite (ZnO-GO). FES-coated ZnO and ZnO-GO using a simplified synthesis procedure follows the literature procedure[35] with certain modifications. For growing ZnO nanorods onto the surface, 62.5 mL of methanol containing 0.01 M [$Zn(Ac)_2$] was kept on a beaker at a temperature of 60 °C under constant stirring. The stirring process is accompanied by dropwise addition of 0.03 M NaOH mixed in 32.5 mL of DI water, under strong stirring for 3 h for uniform growth of ZnO nanoseed. The solution is ultrasonicated for ca. 30 min for enhanced adhesion properties, which can grow in situ to form a thin film by drop casting on a substrate placed on a heated surface of 170 °C. GO was fabricated using the modified Hummer's process with slight modification, discussed elsewhere.[36] The first step in the fabrication of the GO is by choosing its derivative with different chemical properties and sizes best suited for the treatment application, which is detailed in Supplementary S1.[37] The growth of ZnO nanorod was achieved through an 800 mL of DI water solution mixture of 0.025 M zinc nitrate hexahydrate [$(Zn(NO_3))_2\cdot 6H_2O$] and 0.125 M HMTA by ultrasonication for ca. 60 min for homogenization.[38] The patterned ZnO nanorod thin film was obtained by placing thin drop cast ZnO nanoseed film on a substrate in the solution for 2 h at 90 °C in the oven to result in a desired "FES". ZnO-GO was obtained through a process of mixing ZnO nanoseeds with GO solution and grown using a similar procedure as outlined in Supplementary S2. The fabrication and coating of the ZnO/ZnO-GO on the metallic substrate through this simplified process resulted in a large growth area and enhanced performance of FES for the remediation of the dye effluent.

2.4. Spectrometric Studies. Spectrometric analysis for the initial and degradation dye samples are carried out using an Evolution 300 UV−vis spectrophotometer equipped with a long-lifetime xenon flash lamp and extended wavelength-range silicon photodiode detectors. VISIONpro, Thermo Scientific software, was utilized as a control and data manipulation

https://doi.org/10.1021/acsomega.3c03122
ACS Omega 2023, 8, 28615−28627

package for scanning for sample identification, method development, quantitative analysis, etc. The output is taken as samples of size 25 mL each from the photocatalytic reactor every hour and filtered using a 0.22 μm Durapore PVDF membrane filter unit and stored in 15 mL Graduated Centrifuge tubes (Tarsons) in dark containers. The test process lasts for 5 h until complete degradation where each step is repeated, and the samples are stored for further analysis. For the analysis of the absorbance of the samples, 1 mL of samples is analyzed through an UV−vis spectrophotometer. Quantification of the dye was performed at different wavelengths of λ = 596 nm for RB-4 dye, λ = 661 nm for the industrial dye sample, and wavelengths of {λ = (543 nm), (624 nm), (560 nm), and (589 nm)} for various mentioned industrial reactive dyes that form the part of the effluent mixture.

2.5. Adsorption Study. The adsorption capacity of the synthesized FES is determined using known kinetic and isotherm models.[29] A kinetic process based on the Langmuir−Hinshelwood process[39] is used for modeling the generation of electrons and holes in the presence of solar irradiation. Photocatalytic dye degradation reactions follow the Langmuir mechanism, $\frac{dC}{dt} = k_{app} \times C$, upon integration, yields the following relation of $\ln\left(\frac{C_0}{C}\right) = k_{app} \times t$ where $\frac{dC}{dt}$ is the rate of change of dye decoloration with light irradiation, "t" denotes treatment process time (min), and k_{app} represents pseudo-first-order decoloration reaction rate constant (min^{-1}) equal to the slope of the fitting line. The Langmuir−Hinshelwood process is expressed through the first-order equations $C = C_0.\exp(-k_{app}t)$. The reaction rate of decoloration follows the first-order kinetics, and the pseudo-first-order reaction rate constant is determined through the semi-logarithm plot of $\left(\frac{C_0}{C}\right)$ versus time (t). Normalized concentration variation through photocatalysis reaction time can be observed through the straight line, resulting in the constant k_{app} value. For determining the efficiency, the percentage of dye decoloration is obtained using the relation of dye degradation (%) = $[{}^{(C-C_0)}/_{C_0}] \times 100$ where "C_0" and "C" are initial and instantaneous dye concentrations, respectively. The calibration experiments are performed to ascertain the unknown dye concentration correlating with the standard response of the known concentration through a sequential dilution of solutions, ranging from 400 to 0 mg/L at a dilution interval of 50 mg/L.[40]

2.6. Material Characterization. Characterization of the synthesized ZnO and ZnO-GO-based FES is performed using FESEM (Zeiss Supra 40 V, Germany), X-ray diffraction (XRD) technique (PANalytical, Cu Kα, wavelength = 1.5418 Å), Raman spectroscopy (WITec alpha 300, Helium−Neon laser, and wavelength 532 nm), TEM (Titan G2 60-300 KV TEM), FTIR, and EDS analysis, respectively. To quantify the electrochemical properties of the FES, the cyclic voltammetry (CV) technique is utilized. The electrochemical properties are investigated for the redox potential wrt current[41] using CV on the AUTOLAB workstation (PGSTAT302N). It utilizes a three-electrode system with FES as the working electrode, Ag/AgCl (3 M KCl) as the reference electrode, and platinum foil as the counter electrode in 2.5 M Na_2SO_4 aqueous solution.[42,43] The electrode has been developed for half-cell measurements using an earlier defined methodology on an aluminum foil substrate. The CV measurements were recorded in the potential range of −1 to +1 V for a range of scan rates from 10 to 50 mV/s, and all experimental measurements are recorded at room temperature.[44] Electrochemical studies are performed by differing scan rates, referred to as the variation of the potential wrt time.

2.7. Dye Characterization. NMR spectra were recorded on a 500 MHz JEOL NMR spectrometer which is equipped with a ROYAL HFX FGSQ probe that achieves high-precision digital RF and provides crystal clear spectral patterns.[45,46] DMSO-d_6 was taken as the solvent and 15 mg of compound for the NMR analysis. The solution was properly shaken for getting a uniform solution. ^{1}H NMR, ^{13}C NMR, and DEPT-135, 90, and 45 were performed to identify the probable structure of an unknown industrial dye molecule, as shown in Figure 4. The NMR data were processed using JEOL Delta NMR processor (version 5.3.1).

To identify the intermediaries formed during the AOP-based dye degradation process, it was analyzed at regular intervals using advanced chromatographic techniques for identification of separate species. HPLC and liquid chromatography—quadrupole time of flight—MS/MS (LC-QTOF-MS/MS)[47] are utilized to identify the characteristics of the dye-degraded product samples.[48,49] HPLC analysis of the dye samples is performed using Agilent 1260 Infinity II LC System unit equipped with a diode array detector (DAD) and ZORBAX Eclipse Plus C18 column (95 Å, 4.6 × 250 mm, 5 μm, 400 bar pressure limit) along with a ZORBAX semi-preparative guard column hardware which provides higher safety for dye-based effluents. The method developed for the analysis is detailed: methanol concentration in eluent D starts from 10% and reaches 100% in 10 min in a gradient mode, then held constant for 3 min in an isocratic mode, ramped up to 100% in the next 3 min, and is held constant at 10% for the last 4 min, resulting in a total run time of 20 min.

LC-QTOF-MS/MS analyses were performed on an Agilent Technology 1260 HPLC system coupled with an Agilent 6200 series TOF/6500 series Q-TOF 10.1 (48.0) (Agilent Technologies) and a DAD on a C-18 column (2.1 × 50 mm, 2.5 μm). The column was kept at room temperature for an injection volume of 50 μL and an eluent flow rate of 1.0 mL/min. The mobile phase consists of HPLC grade water (B) with gradient elution (pH adjusted to 4 by adding formic acid) and methanol (A). A Q-TOF mass spectrometer was operated in the positive electrospray ionization (ESI) mode at high resolution (4 GHz) with a resolving power, ranging from 9700 to 18,000 for the m/z 100−1600, respectively. The MS parameters used are drying gas flow rate = 12 L/min at 355 °C, nebulizer pressure = 35 psi, and fragmentor voltage = 110 V with the V_{cap} voltage of 3500 V. To improve the mass measurement accuracy, a reference mixture from Agilent Technologies (part number: G1969-85001) has been introduced via a secondary ESI needle at a flow rate of 0.1 mL/min.

3. RESULTS AND DISCUSSION

3.1. Synthesis and Characterization of ZnO Nanorod/ZnO-GO Nanocomposite-Based Filter Element Substrates. Synthesis of ZnO/ZnO-GO-based FES nanocomposites was carried out with modifications in the previously reported methods.[11,20] Briefly, ZnO nanoseed was obtained using a simplified synthesis procedure for uniform growth and enhanced adhesion properties, outlined in the Material Characterization section. Following this, the solution is drop

https://doi.org/10.1021/acsomega.3c03122
ACS Omega 2023, 8, 28615−28627

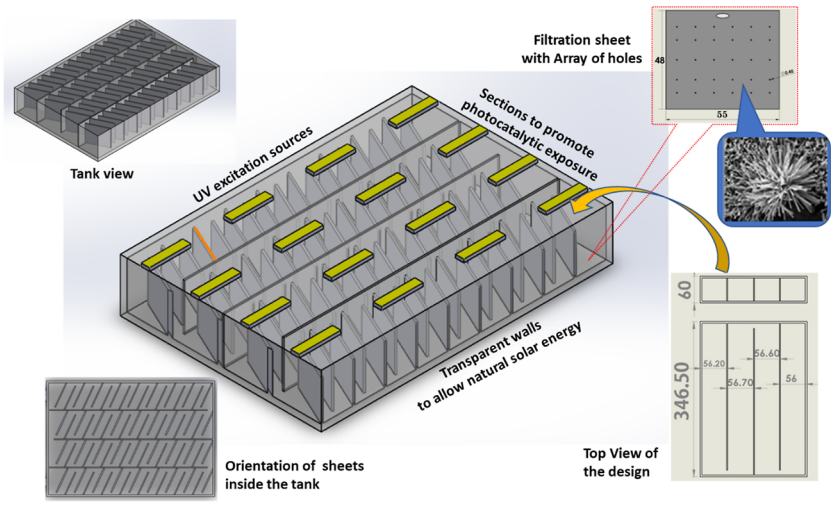

Figure 1. Cross-sectional view of the prototype dye-wastewater treatment pilot unit using ZnO nanorod-coated FESs acting as the photocatalytic element for the remediation unit comprising the combination processes of the treatment operations. Design of the photocatalytic reactor having top and sides transparent to capture the maximum solar irradiation which promotes the exposure on the FES for a faster catalytic process (upper left inset image shows the tank view which is rectangular having dimensions of 570 × 480 × 1.5 mm^3, lower left inset image shows the orientation of the FES-coated sheets to maximize the sunlight exposure to the sunlight, lower right inset image details the top view of the reactor, and upper right inset image shows the design of the FES-coated plate having equidistant holes for the effective treatment process and FESEM image of the ZnO nanorod structure of the photocatalyst).

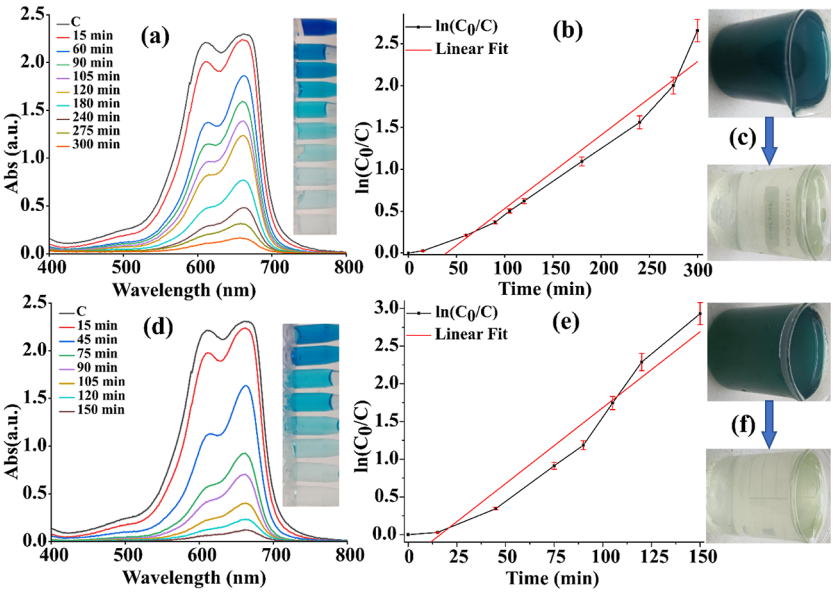

Figure 2. Variation of the output fluorescence emission spectra of (a) ZnO FES-based solar-induced remediation of the industrial dye wastewater, (b) time variation of the logarithmic normalized concentration for the remediation process for the industrial wastewater (λ = 661 nm), (c) decolorization effect on the initial industrial dye wastewater using ZnO FES after 5 h where the arrow indicates the degradation from the initial to final remediation product during the experimental study in the plant and (d) ZnO-GO FES-based solar-induced remediation of the industrial dye wastewater, (e) time variation of the logarithmic normalized concentration for the remediation process for the industrial wastewater (λ = 661 nm), and (f) decolorization effect on the initial industrial dye wastewater using ZnO-GO FES after 5 h where the arrow indicates the degradation from the initial to final remediation during the experimental study in the plant.

cast on a heated substrate surface and grown for uniform ZnO nanorod structures. GO-based ZnO-GO FES is fabricated using the modified Hummer's process with slight modification, discussed elsewhere.[50] ZnO-GO was obtained through a process of mixing ZnO nanoseeds with GO solution and grown using a similar procedure, outlined in Material Characterization section. Fabrication and coating of ZnO-GO nanocomposites on the substrate resulted in a large growth area and enhanced performance of the FES. The characterization of the synthesized FES was carried out using FE-SEM, TEM, FTIR XRD, and EDS techniques and is detailed in the Supporting Information section.

The surface morphology and size analysis of the synthesized FES was performed using FE-SEM and TEM, as detailed in Figures S9−S11. Figures S9 and S10 show the growth of ZnO and ZnO-GO nanorods on the FES with lower and higher magnifications analyzed to an average length of 200 ± 50 nm and length of 2 ± 0.6 μm with a diameter of 400 ± 150 nm,

https://doi.org/10.1021/acsomega.3c03122
ACS Omega 2023, 8, 28615−28627

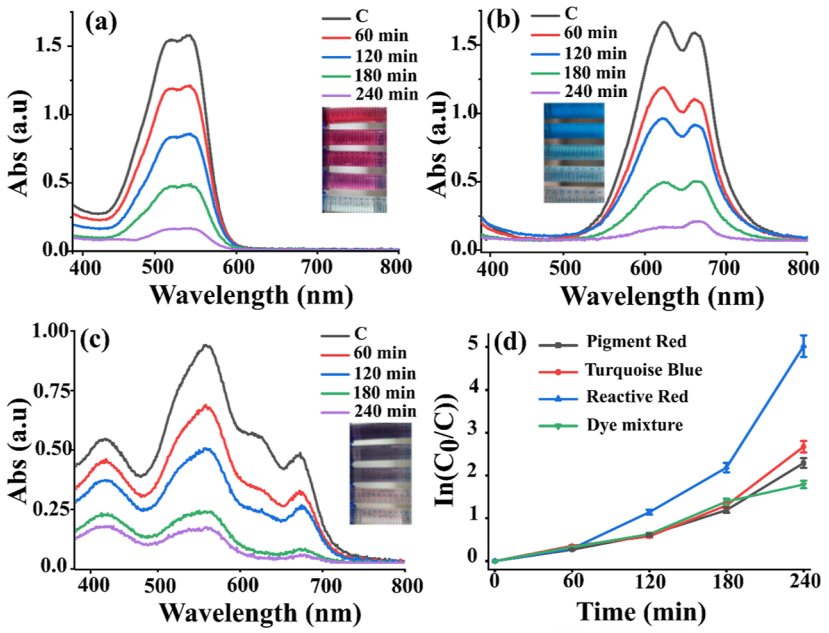

Figure 3. Variation of the output UV−vis absorption spectra of ZnO FES-based solar-induced remediation of the (a) reactive red dye (λ = 543 nm), (b) turquoise blue (λ = 624 nm), (c) dye mixture of pigment red, turquoise blue, reactive red, reactive blue, and reactive yellow dyes { λ = (543 nm), (624 nm), (560 nm), (589 nm)}, and (d) comparative plot of the time variation of the logarithmic normalized concentration for the remediation process for the various industrial reactive dyes {λ = (543 nm), (624 nm), (560 nm), [(543 nm), (624 nm), (560 nm), (589 nm)]} indicates the degradation from the initial to final remediation product using the ZnO-coated filter element substrate.

respectively. Figure S11 shows the internal morphology, confirming the growth of the ZnO on the GO sheets which is visible through the interfacial contact. Selective area electron diffraction analysis (SAED) shows a good amount of crystallinity present through the visible polycrystalline structure. Figure S12 shows the XRD analysis for the characteristic peaks of the wurtzite-type crystal structures of ZnO and the characteristic (001) peak of graphene oxide (GO)[51] and (001) peak of GO shifts, which are mainly due to the heterojunction effect between ZnO and GO.[52] The reason for the peak shift and decrease in intensity is mainly attributed to the exfoliation of the GO sheets which were stacked earlier in the pure form of GO. The FTIR spectra of ZnO-GO with peaks at 1625 cm^{-1} correspond to the C═O stretching bond, which gets shifted from 1617 cm^{-1} in the case of pure GO due to composite formation.[51] The Raman spectra show two characteristic peaks at 1350 and 1580 cm^{-1} corresponding to the D band and G band of GO,[53] which represent in and out-of-plane sp^3- and sp^2-hybridized carbon atoms created due to acid exfoliation of the graphite.[54]

3.2. Photocatalytic Pilot-Scale Dye Remediation Unit. The dye remediation process was carried out through the designed FES coated with ZnO in the photocatalytic reactor, as illustrated in Figure 1 and detailed in Supplementary S1. Briefly, the pilot-scale photocatalytic reactor is designed to accommodate serially placed perforated FES made from ZnO-coated stainless steel (SS) sheet panels on two sequential chambers which are divided into four parallel sections and are transparent to incident solar radiation. The effluent passes through each unit on the serpentine flow path through perforated coated sheets for maximum effluent contact time, thereby maximizing the catalytic treatment process. The galvanized SS sheets were custom-made for the reactor with equidistant holes over the whole surface area of the sheet having dimensions of 570 × 480 × 1.5 mm^3. The dye remediation process through the photocatalytic tank reactor is designed for a 4 h cycle. Results of the degradation process are detailed in subsequent sections, with the basic conclusion that the photocatalytic process cleaves/degrades the dye molecule into smaller fragments which either decompose as H_2O and CO_2 and are filtered through carbon filtration processes.[55]

3.3. Photocatalytic Dye Remediation Using the Filter Element Substrate. To ascertain the process of photocatalytic remediation for industrial dye-effluent wastewater, a known RB-4 dye-based aqueous solution and the wastewater obtained from various industrial reactive dyes were used for the experimental studies in this section. Dye degradation parameters were evaluated using UV−vis absorption analysis for both ZnO and ZnO-GO-based FES. Figure 2 shows the solar light-induced industrial dye remediation through the UV−vis-based emission spectra with the rate of degradation kinetics along with the initial and final remediation products. As shown in Figure 2a, upon treatment of industrial wastewater with ZnO, a time-dependent degradation of the dye present in the wastewater was observed. Initially, the dye-containing wastewater shows the presence of two intense bands at 611 and 661 nm, respectively, in the UV−vis spectrum. The appearance of such bands usually indicates the presence of the dye in aggregated states with H-aggregates giving a blue-shifted band while J-aggregates give a red-shifted band.[56] The degradation kinetics was followed for 5 h which showed nearly complete removal of the dye both through the absorption band and visually (see the inset for visual results). Further analysis of degradation (Figure 2b) yielded a pseudo-first-order reaction kinetics with a rate constant (k_{app}) of 0.0083 min^{-1}. Using ZnO-GO FES for the same experiment, as shown in Figure 2d, the dye degradation in the industrial wastewater was much faster with near completion of the dye degradation in 150 min. Further analysis of the degradation rate constant value of 0.02015 min^{-1} shows an increase by a

https://doi.org/10.1021/acsomega.3c03122
ACS Omega 2023, 8, 28615−28627

factor of 2.43 when compared with the degradation kinetics of ZnO. This enhanced rate constant of dye degradation depicts increased photocatalysis and effective remediation of the industrial dye wastewater.

The degradation experiments were also performed using reactive dyes in the textile industry such as pigment red, turquoise blue, reactive red, and a dye mixture of pigment red, turquoise blue, reactive red, reactive blue, and reactive yellow dyes to demonstrate the generality and wide scope of use of the newly synthesized ZnO FES. A representative example is shown in Figure 3a which shows a time-dependent decrease in the absorption maximum (λ = 543 nm) of the dye pigment red. Near completion of the dye removal was achieved in 4 h through Figure 3 which can be seen both visually and through the UV−vis analysis. Similar observations were obtained with other reactive dyes (turquoise blue, reactive red, and a dye mixture of pigment red, turquoise blue, reactive red, reactive blue, and reactive yellow dyes) which showed >95% degradation within 4 h (see Supporting Information Figures S1−S2 and Table S1 for additional details). A comparative plot of degradation kinetic rates is shown in Figure 3d, which demonstrates its dye degradation efficiency in varied systems.

A similar study is performed on the control RB-4 dye sample due to the known dye molecular structure and higher efficiency for HPLC processing with similarity in composition to the industrial textile dye. Figure S1 shows the complete degradation through the absorption spectra showing a pseudo-first-order behavior for both ZnO and ZnO-GO FES having corresponding k_{app} and R^2 values of 0.01084 and 0.01883 min^{-1} and 0.96 and 0.93, respectively.[57] Absorption analysis of the synthesized ZnO and ZnO-GO-based FES[33] shows the lateral shift in the absorbance peak of ZnO due to a change in the nanostructure from 354 to 365 nm as GO absorbs the whole visible light spectrum, which is due to the complete absorption of the whole visible light spectrum. This leads to a higher overall absorption capacity of the ZnO-GO which helps improve the photocatalytic process activity for dye wastewater by utilizing sunlight through the creation of electron-hole pairs. The resultant band gap energy for ZnO and ZnO-GO was found to decrease from 3.12 and 3.06 eV, respectively, due to the charge carrier concentration on the GO sheet.[58] Quantification of the photocatalytic remediation process is performed using a univariate calibration model which provides the relationship between the characteristic response with the concentration of the dye present in the wastewater sample. Supplementary Figures S14−S15 and Table S5 show a consistent fit curve for the change in the concentration of industrial reactive dyes, providing high prediction and complete degradation achieved through the synthesized FES and consistent curve fit having R^2 values from 0.97 to 0.999.

3.4. Statistical Analysis. Statistical analysis of the degradation process of industrial wastewater yielded a pseudo-first-order reaction kinetics having a rate constant (k_{app}) value of 0.0083 min^{-1}, which increases by a factor of 2.43 to a value of 0.02015 min^{-1} using ZnO-GO FES for the same experiment, as shown in Figure 2. The details of the various statistical parameter obtained are given in Table 1. Various other industrial dyes are used for the ZnO FES-based photocatalytic experimental studies following the first-order rate constant behavior, as detailed in Table 2. The results show a significantly less residual sum of square values with a better fit of the experimental values and similar slopes for all the industrial dye samples showing consistent behavior of the FES for the degradation process except for reactive red dye.

Table 1. Statistical Analysis Result of the Kinetics Obtained for Time Variation of the Logarithmic Normalized Concentration for the Remediation Process for the Industrial Wastewater (λ = 661 nm) Dyes

	industrial dye wastewater	
model parameters	ZnO FES	ZnO-GO FES
intercept	−0.3468 ± 0.12746	−0.3318 ± 0.17315
slope	0.00878 ± 7.06437 × 10^{-4}	0.02015 ± 0.00194
residual sum of squares	0.27891	0.42566
Pearson's r	0.97808	0.97337
R-square (COD)	0.95664	0.94746
adj. R-square	0.95045	0.9387

3.5. Characterization of Industrial Reactive Dyes and Properties. For textile-based applications, anthraquinone-derived reactive dyes with a quinoid ring as the chromosphere are commonly utilized. Commercial reactive dyes commonly used in textile industries were obtained from the Jaipur Industrial Park. RB-4 dye [Figure 4a and Table S2] is used as a known dye in experiments involving degradation, which is highly soluble in water and emits a specific color. The industrial CRB was analyzed via 2D NMR spectra (as detailed in Figure 4b and Table S2). NMR spectroscopy was utilized to get insights into the structure and characterization of CRB dye using one- and two-dimensional techniques such as ^{1}H, ^{13}C, COSY, and HSQC (see Figures S3−S8 for probable chemical shifts). The proton signals at 13.1, 10.8, and 8.7 ppm integrating one each likely belongs to the −NH and −COOH functionalities present in the structure shown in Figure 4b. The two protons showing a chemical shift value of 3.9 and 3.5 ppm belong to two distinct CH_2 protons which are conspicuously seen in DEPT-135 spectrum (Figure S6). Partial $^{1}H-^{1}H$ correlation spectroscopy (COSY) data depicting the aromatic region (Figure S7) showed five scalar cross peaks consistent with the structure shown in Figure 4b. Both distortionless enhancement by polarization transfer (DEPT) and heteronuclear multiple quantum correlation (HMQC) spectra showed the presence of six resonances belonging to carbons directly attached to hydrogens in the aromatic region (Figures S6 and S8). The acidic and carbonyl carbons show chemical shift values of 177.2 and ∼164.6 ppm while the aliphatic carbons show chemical shifts of 59.8 and 55.4 ppm, respectively.

CV analysis is performed to study the redox reaction process of the dye species with the FES and chart the significant effect of the adsorption on the surface, evaluated through the isotherm studies. Figure 5 shows the CV profiles for FES at different scan rates within the fixed potential window of −1 to +1 V. The results show enhanced reduction and oxidation peaks at 50 mV/s showing increased photocurrent densities and better charge transition behavior of the photocatalyst.[59] Higher redox peaks for the ZnO-GO at 50 mV/s compared to that for ZnO at 30 mV/s shows good charge-transfer performance of the ZnO FES for the photocatalytic degradation process.[60] An enhanced redox peak of ZnO-GO shows a higher peak current at different potentials ascribing to good photocatalytic activity and higher capacitance of the FES due to the impact created by GO on the ZnO polarity.

https://doi.org/10.1021/acsomega.3c03122
ACS Omega 2023, 8, 28615−28627

Table 2. Statistical Analysis Result of the Kinetics Obtained for Various Industrial Dyes Used for the Remediation Process: (a) Industrial Dye Wastewater, (b) Reactive Blue-4 Dye, (c) CRB Dye, (d) Pigment Red, (e) Turquoise Blue, (f) Reactive Red, (d) Dye Mixture of (Pigment Red, Turquoise Blue, Reactive Red, Reactive Blue, and Reactive Yellow) Dyes

	dyes					
parameters	RB-4	CRB	pigment red	turquoise blue	reactive red	dye mixture
intercept	−0.34 ± 0.27	−0.07 ± 0.32	−0.23 ± 0.24	−0.28 ± 0.32	−0.66 ± 0.66	−0.11 ± 0.11
slope	0.01 ± 0.01	0.01 ± 0.01	0.01 ± 0.001	0.01 ± 0.01	0.02 ± 0.01	0.008 ± 7.6 × 10^{-4}
residual sum of squares	0.54	0.80	0.28	0.53	2.208	0.06
Pearson's *r*	0.97	0.96	0.96	0.94	0.93	0.99
R-square (COD)	0.93	0.92	0.92	0.88	0.87	0.97
adj. *R*-square	0.92	0.89	0.89	0.845	0.82	0.96

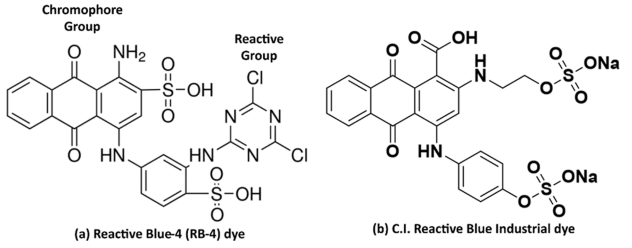

Figure 4. Chemical structure of (a) reactive blue-4 (RB-4) (empirical formula: $C_{23}H_{14}Cl_2N_6O_8S_2$ and molecular weight: 637.43) consisting of 2-amino groups and a sulfonate group and (b) CRB industrial dye probable structure obtained through 2D NMR analysis [detailed through the Supplementary Section S1 (5)].

3.6. Dye Remediation Analysis Using HPLC. HPLC analysis was performed for determining the nature of the degradation compounds during the remediation process. The reverse phase separation mode without an ion-pairing agent was employed for establishing the HPLC method.

Figure 6 shows the 3D HPLC chromatogram for quantitative identification through the separation of the RB-4 and industrial CRB dye and degradation compounds at the peak absorption wavelengths (λ = 598 and 589 nm, respectively) for an initial concentration of 400 mg/L. A significant peak is monitored at a retention time (t_R) of 9.8 min along with four other minor peaks at 7.4, 8.0, 8.4, and 12.3 min for the initial dye sample. The major peak of the chromatogram obtained at t_R 9.8 min showed a significant decrease in the absorbance intensity of the compound species. Intermediaries visible through the HPLC chromatogram correlate with the UV−vis results obtained in (2) and Supplementary Section S1. The peak elution is visibly shifted to a t_R of 12 min due to the formation of other species (metabolic) through possible dimerization or association of the degraded dye compounds. Various other metabolic start appearing at the t_R 2.2−2.8 min, which suggests the formation of small impurities suggesting the formation of more polar molecules. Similarly, for industrial CRB dye initial dye sample shows characteristic peaks at t_R of 8.7 and 10 min, showing significant absorbance due to the presence of individual compounds, while the peak at t_R of 9.5 min shows the presence of impurities in the sample. The degradation compounds show a partial shift due to the formation of the new compounds and the presence of small metabolite at t_R 2.2−2.8 min which suggests the formation of small impurities through more polar molecules. HPLC chromatogram spectra concurrently vanish in 5 h, showing complete (≈99%) degradation under solar irradiation-induced photocatalysis.

3.7. Design of Probable Degradation Mechanism Using Liquid Chromatography-Mass Spectrometry (LC-QTOF-MS/MS). A detailed analysis of dye degradation behavior was performed using LC-QTOF-MS/MS to identify the intermediates formed during the dye remediation process. Preliminary experimental work was carried out for the determination of the degradation compounds using positive-ion mode MS.[61] The positive-ion mode resulted in higher sensitivity with specific signals obtained for certain proton acceptor groups. Various literature reports suggested the formation of mono- and di-sulfonate adducts (with sodium counterion) along with DI molecular ions, i.e., $[M + H]^+$ or $[M + 2H]^{2+}$ or $[M + 2H - Na]^{2+}$. A generalized expression, given by $[M + (x + y)\cdot H - y\cdot Na]^{x+}$ predicts the fragment ions, where $x > y$ and x or $(x + y)$ = total acid groups.

Analyzing the predicted MS fragment ions is performed only for major m/z peak values for each degraded sample using isotope modeling and detailed through supplementary Figure S20. QTOF-MS/MS data obtained for the degradation dye

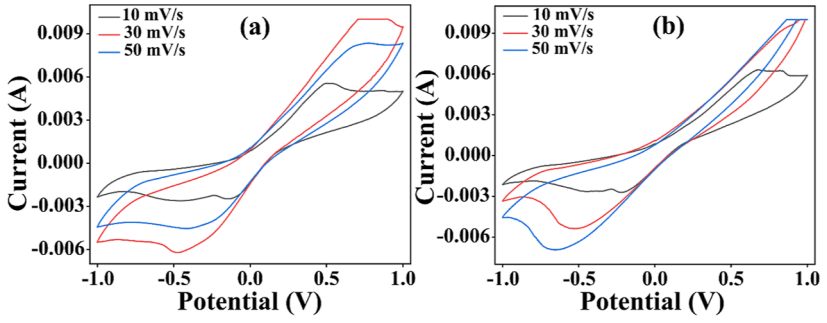

Figure 5. (a) Comparison of the CV profiles of ZnO nanorod-based FES at different scan rates of 10, 30, and 50 mV/s within the fixed potential window between −1 and +1 V. (b) Comparison of the CV profiles of ZnO-GO nanocomposite-based FES at different scan rates of 10, 30, and 50 mV/s within the fixed potential window between −1 and +1 V.

https://doi.org/10.1021/acsomega.3c03122
ACS Omega 2023, 8, 28615−28627

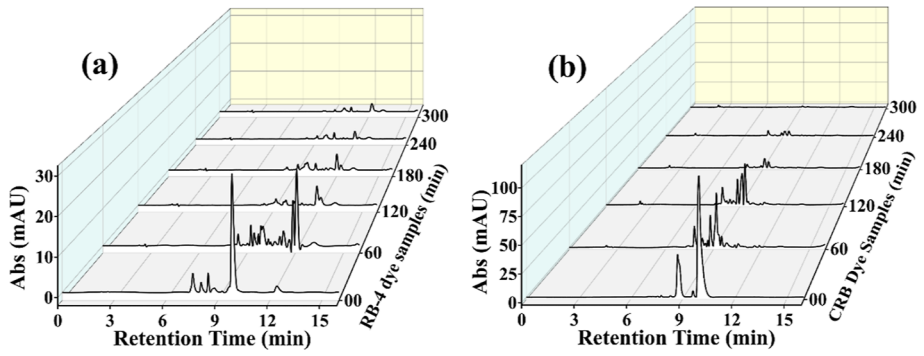

Figure 6. 3D HPLC chromatogram of the initial dye samples of concentration 400 mg/L in the aqueous medium and the subsequent degradation dye samples at 1 h time intervals each for 5 h i.e. 60 min intervals for (a) reactive-blue 4 (RB-4) dye at the peak absorption wavelength (λ = 598 nm) and (b) CRB dye (CRB) peak absorption wavelength (λ = 589 nm).

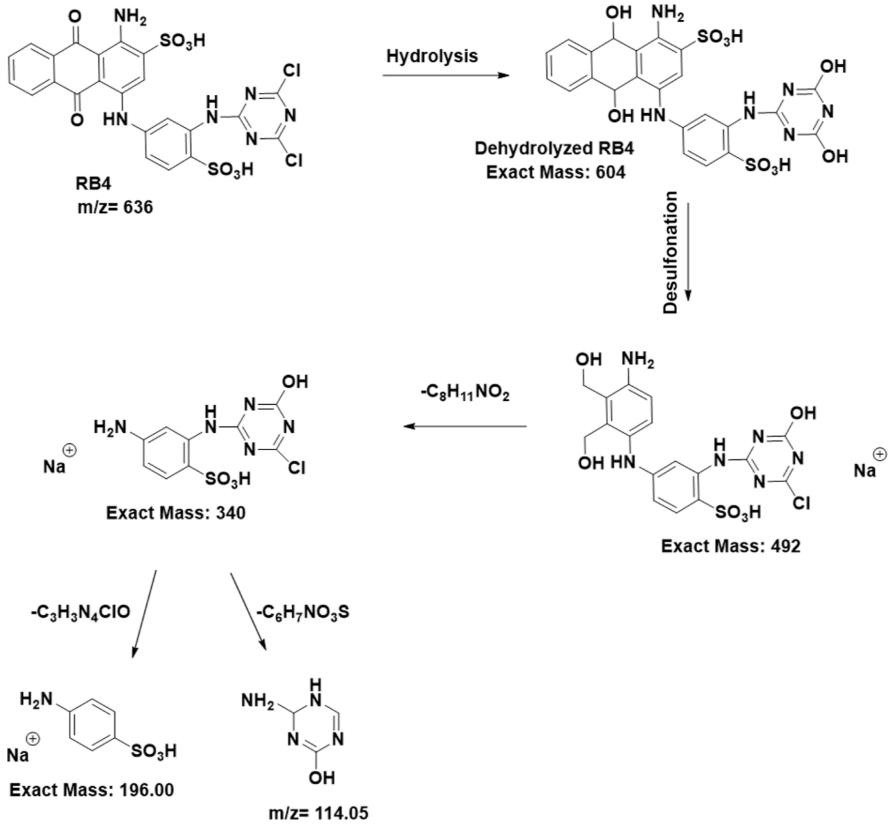

Figure 7. Plausible successive fragmentation mechanism for designing the pathway due to mineralization of the RB-4 dyes molecule into degraded compound identified using LC/QTOF-MS/MS.

samples show an appreciable decrease in the chromophoric components at corresponding retention time (t_R) of 9.7, 10.8, and 13.8 min. Major peaks obtained at t_R = 9.7 min are m/z 605, 492, 340, 198, and 114, while for t_R = 10.8 and 13.8 min, corresponding m/z obtained are 566, 492, 340, 114, 492, and 114, respectively. A detailed analysis resulted in the observation of the major fragments at m/z 605, 492, 340, 198, and 114. The parent ion peak obtained at m/z 605 corresponds to a degraded fragment of the RB-4 dye molecule into the di-hydrolyzed form, which upon forming an H-bond with a water molecule imparts distinct coloration. The targeting of free radicals during the process of photocatalytic degradation is achieved by undergoing reduction of the target molecule which cleaves into small fragments of $-SO_3H$, $-COOH$, and $-OH$, ions. The detailed mechanism of this process is discussed based on the obtained fragmentation pattern in Figure 7. A degradation process via reduction, elimination, and bond cleavage through radical attack occurs in the forward direction to smaller m/z ratios. The chromophoric group loses its property in the visible range when the group dissociates through the reduction of the RB-4 dye molecules. Fragments obtained at m/z 492 correspond to the chromophoric group while m/z 198 and 114 belong to corresponding small organic compounds of the dye molecule obtained through the degradation process.

Similarly, QTOF-MS/MS data obtained for CRB dye degradation samples show a linear decrease in the chromophoric component. The major peak elution at t_R 8.7 and 10 min shows highly similar mass fragmentation patterns of m/z 564, 408, 340, 252, 224 and 480, 451, 317, respectively, due to

https://doi.org/10.1021/acsomega.3c03122
ACS Omega 2023, 8, 28615−28627

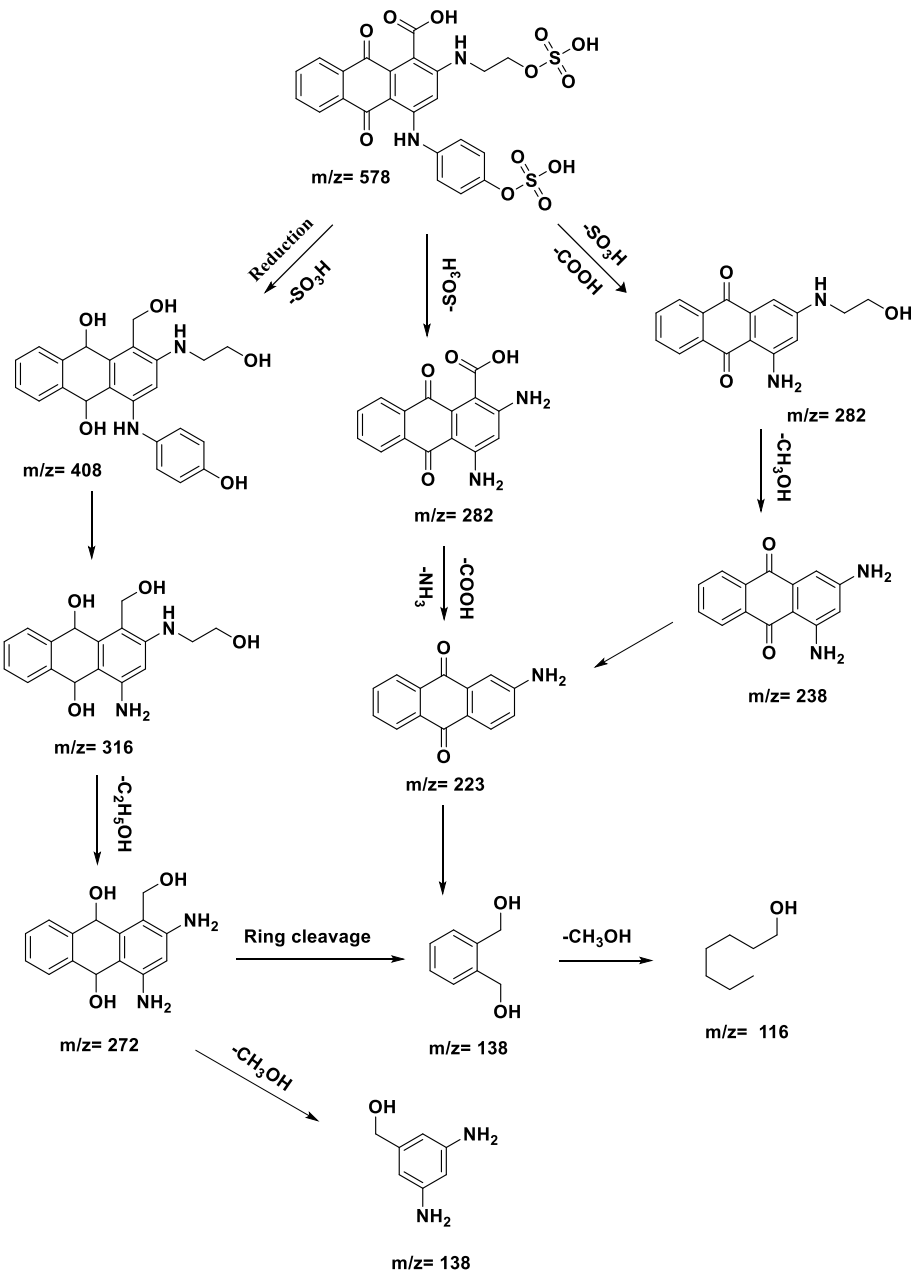

Figure 8. Plausible successive fragmentation mechanism for designing the pathway due to mineralization of the industrial CRB dye molecule into degraded compounds identified using LC/QTOF-MS/MS.

fragmentation of the original dye molecule through cleaving. The separation of the bridging group results in a plausible fragmented molecule corresponding to m/z 282. During the process of degradation, certain groups like $-SO_3H$, $-C00H$, $-CH_3OH$, $-C_2H_5OH$, $-NH_3$, and so forth are eliminated, resulting in the formation of possible intermediaries. The proposed remediation mechanism, as shown in Figure 8, presents various probable pathways obtained from free radical $^{\bullet}OH$ induced degradation of the CRB dye wastewater. Various intermediaries are formed by reductive cleavage of the $-SO_3H$ group by detaching to form an H-bond with water and separation of the small acidic groups. Small molecules which are more stable are oxidized in the form of CO_2 and H_2O from the dissociation of the acidic $-COOH$ and amino group which further result in the formation of NH_3. It can also be observed that the slightly acidic pH (~6.8) leads to dissociation and fragmentation of small molecules into gaseous residues and compounds with alcoholic properties.

3.8. Reusability and Regeneration of FES. A study on the reusability and regeneration of the FES is performed to examine the extent of the degradation of the substrate following the photocatalytic process in the pilot treatment plant. FES has been used consecutively for 11 cycles during which remediation of the dye compound efficiency decreases to the minimum threshold value, as shown in Figure 9. After each degradation process cycle, the FES is washed with DI water, sonicated for 5 min, and kept in DI water for 2 h under stirring. The efficiency of the degradation process remains (>90%) for four cycles and at an acceptable level (>80%) for six cycles. The dye remediation performance degrades (<80%) and crosses the lower threshold level of 50% at the end of the 11th cycle due to blockage of the active sites of the

https://doi.org/10.1021/acsomega.3c03122
ACS Omega 2023, 8, 28615−28627

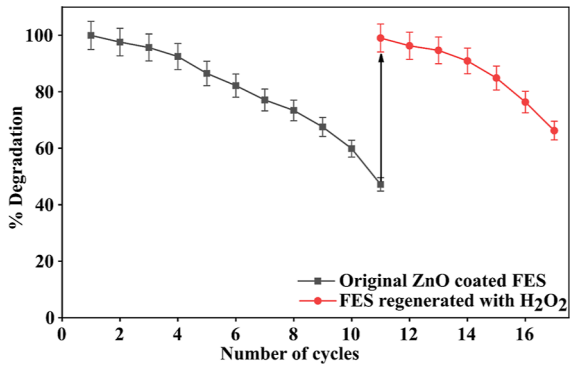

Figure 9. Reusability and regeneration analysis of the ZnO photocatalyst-based FES used in the field treatment plant unit detailing its usability for the remediation process and showing a gradual decrease in the degradation capability. FES regenerated using the defined procedure of H_2O_2 and UV irradiation restores the degradation capacity of the FES through the removal of adsorbed dye from the top surface.

photocatalysts through adsorbed dye molecules. The regeneration process follows the procedure

a FES is placed in a solution mixture of 1 M H_2O_2 in an UV-irradiated source for 8 h.
b FES is treated with DI water upon completion of the process.[62]

UV irradiations with wavelengths lower than 300 nm help in the generation of hydroxyl radicals (•OH) which removes the dye from the active sites, resulting in the formation of •OH from H_2O_2.

$$H_2O_2 + h\nu \rightarrow 2^{\bullet}OH \quad (1)$$

This process of treatment restores the FES performance to its original characteristic degradation efficiency of 99% after completion of the regeneration process. After regeneration, FES can be reused for a limited number of cycles of six until it crosses the lower threshold efficiency of 60% dye removal.

3.9. Free-Radical-Induced Photocatalytic Remediation Mechanism. The process of dye remediation through photocatalysis is based on a photoreaction mechanism, in which the specific photocatalyst under solar irradiation initiates the chemical transformation process by absorbing the solar light photons. The photocatalytic mechanism is accomplished by the formation of electron-hole pairs, initiating the transformation through interfacial contact followed by the redox reaction with FES and evolution of end-products.[63] The FES-induced remediation process follows the principle of trapping the holes (h^+) generated through pairs of electrons and holes created by light irradiation on surface defects. The surface defects react to produce reactive dye species which are further degraded by recombination with the photogenerated holes through the mechanism of chemisorption. For visible light-based oxidation, the dye absorbs the light photons by producing electrons e^-_{CB} on the conduction band. Absorption of the conduction band electron follows the process of oxygen ion sorption where the oxygen is reduced to its oxidized form. The generated photo-holes neutralize the hydroxyl group to form hydroxyl radical (•OH), while the proton neutralizes the oxide radical $O2^{\bullet-}$ to form the hydroperoxyl radical which reduces to form transient hydrogen peroxide along with the dismutation of oxygen. Hydrogen peroxide in the reaction with the e^-_{CB} leads to the decomposition into hydroxyl ion and to hydroxyl radical with the second reduction of oxygen. The reactive dye species oxidize via direct successive attack of the hydroxyl radicals, leading to the formation of CO_2 and H_2O. Direct oxidation of reactive dyes in the combination of h^+ results in the formation of oxidation species and complete degradation of dyes through the mechanism shown in Figure 10 and detailed in Supplementary S1 in eqs 2−9 and 10−18. The objective of using ZnO as a photocatalyst for the degradation/remediation of industrial effluents as a major intervention toward an advanced treatment process is achieved.

4. CONCLUSIONS

This work details the AOP-induced remediation of industrial dyes and predicts the intermediaries formed during the degradation process through mass spectrometric analysis. A simple and efficient design of the ZnO and ZnO-GO-coated FES photocatalyst using the solvothermal process for a Pilot

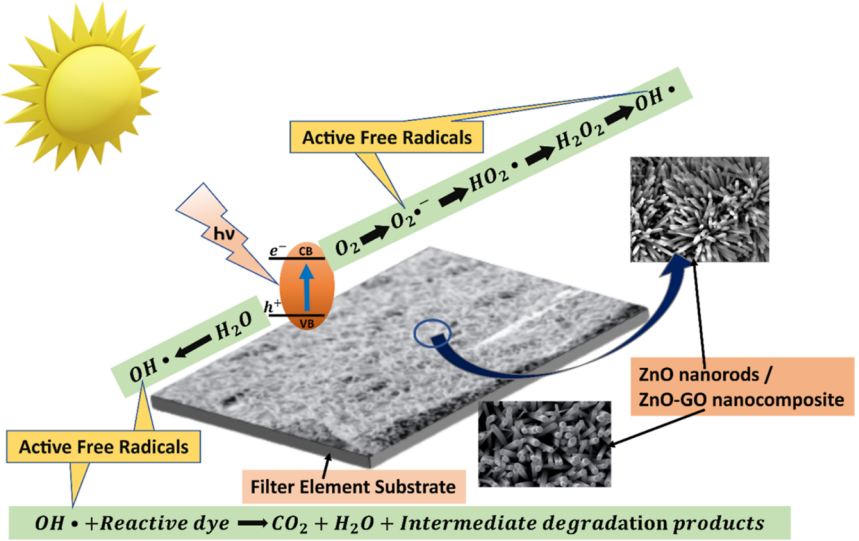

Figure 10. Schematic diagram representing the free-radical-induced decolorization mechanism of industrial reactive dye-based wastewater using FES as a photocatalyst under solar irradiation, resulting in the formation of the intermediate degradation products.

https://doi.org/10.1021/acsomega.3c03122
ACS Omega 2023, 8, 28615−28627

scale treatment plant is utilized for the effective remediation of the industrial dye wastewater. The designed FES resulted in a faster, more effective, and complete degradation process with high-rate kinetics and provides the solar irradiation-based sustainable technology for complete mineralization of the dye effluent. The ZnO-coated FES provides a simple and effective solution for an industrial-scale approach toward the process of dye quenching which is further ratified with HPLC to correlate with molecular degradation. LC−MS and NMR are utilized to obtain the mass information of the degradation compounds and provide a powerful tool for the prediction of the intermediate ion structure used further for correlation-based studies. A detailed study of the regeneration and reusability of the FES presented a sustainable immobilized approach for treatment operations. This study highlights the usefulness of an innovative FES-based reactor design for the development of an efficient visible-light photocatalyst for the remediation of industrial dye wastewater and quantifies the dye degradation based on molecular analysis using various spectral studies.

■ ASSOCIATED CONTENT

Data Availability Statement

All data generated or analyzed during this study are included in this published article (and its Supporting Information files) and are available from the corresponding author upon reasonable request.

Supporting Information

The Supporting Information is available free of charge at https://pubs.acs.org/doi/10.1021/acsomega.3c03122.

Photocatalytic reactor design specification and working; photocatalytic remediation studies of the reactive blue-4 dye and industrial CRB dye; experimental dye properties; 1D and 2D NMR studies of the RB-4 and CRB dyes; results of the characterization of the ZnO and ZnO-GO-coated FES using FESEM, TEM, XDR, FTIR, Raman, EDS, and CV studies; univariate calibration studies on the industrial reactive dyes; HPLC study; LC-QTOF-MS/MS; free-radical-induced photocatalytic remediation mechanism using ZnO and ZnO-GO FES; and synthesis of ZnO and ZnO-GO FES (PDF)

■ AUTHOR INFORMATION

Corresponding Author

Shantanu Bhattacharya − *Department of Mechanical Engineering, Indian Institute of Technology Kanpur, Kanpur 208016 Uttar Pradesh, India;* orcid.org/0000-0002-7902-2119; Email: bhattacs@iitk.ac.in

Authors

Kirtiman Singh − *Microsystems Fabrication Lab, Department of Design, Indian Institute of Technology Kanpur, Kanpur 208016 Uttar Pradesh, India;* orcid.org/0000-0001-9012-9905

Shiwangi Maurya − *Department of Chemistry, Indian Institute of Technology Kanpur, Kanpur 208016 Uttar Pradesh, India*

Surabhi Gupta − *Department of Medicinal Chemistry, National Institute of Pharmaceutical Education and Research-Raebareli, Lucknow 226002 Uttar Pradesh, India*

Nihar Ranjan − *Department of Medicinal Chemistry, National Institute of Pharmaceutical Education and Research-Raebareli, Lucknow 226002 Uttar Pradesh, India;* orcid.org/0000-0003-3581-4605

Gurunath Ramanathan − *Department of Chemistry, Indian Institute of Technology Kanpur, Kanpur 208016 Uttar Pradesh, India;* orcid.org/0000-0003-4627-1677

Complete contact information is available at: https://pubs.acs.org/10.1021/acsomega.3c03122

Author Contributions

K.S.: experiment design, establishment of protocols, conducted the experiments, performed UV−vis, CV, HPLC, MS experiment and analysis, mechanistic studies, original draft of the manuscript, review, and editing. S.M.: conducted MS analysis and review. S.G.: conducted the repeat HPLC and QTOF-MS/MS experiments and NMR analysis. N.R.: NMR analysis, manuscript revision, and editing. G.R.: supervision and review of work. S.B.: conceptualization of the plant and experimental studies, reviewing, editing the manuscript, and managing the funding for this work. All work was carried out at the Microsystem Fabrication Lab, Department of Mechanical Engineering and Department of Chemistry, IIT Kanpur and at the Department of Medicinal Chemistry, National Institute of Pharmaceutical Education and Research, Raebareli, India.

Notes

The authors declare no competing financial interest.

■ ACKNOWLEDGMENTS

This work was funded by Abdul Kalam Technology Innovation National Fellowship, Indian National Academy of Engineering (grant no. INAE/212/AKF/22). The authors are grateful to Department of Medicinal Chemistry, National Institute of Pharmaceutical Education and Research, Raebareli for providing the characterization facilities.

■ REFERENCES

(1) Jo, W.-K.; Tayade, R. J. Recent Developments in Photocatalytic Dye Degradation upon Irradiation with Energy-Efficient Light Emitting Diodes. *Chin. J. Catal.* **2014**, *35*, 1781−1792.

(2) Hossain, M. S.; Das, S. C.; Islam, J. M. M.; Al Mamun, M. A.; Khan, M. A. Reuse of Textile Mill ETP Sludge in Environmental Friendly Bricks—Effect of Gamma Radiation. *Radiat. Phys. Chem.* **2018**, *151*, 77−83.

(3) Pinheiro, H. M.; Touraud, E.; Thomas, O. Aromatic Amines from Azo Dye Reduction: Status Review with Emphasis on Direct UV Spectrophotometric Detection in Textile Industry Wastewaters. *Dyes Pigm.* **2004**, *61*, 121−139.

(4) Benkhaya, S.; M'rabet, S.; El Harfi, A. A Review on Classifications, Recent Synthesis and Applications of Textile Dyes. *Inorg. Chem. Commun.* **2020**, *115*, 107891.

(5) Raj, S.; Singh, H.; Bhattacharya, J. Treatment of Textile Industry Wastewater Based on Coagulation-Flocculation Aided Sedimentation Followed by Adsorption: Process Studies in an Industrial Ecology Concept. *Sci. Total Environ.* **2023**, *857*, 159464.

(6) Zampeta, C.; Bertaki, K.; Triantaphyllidou, I.-E.; Frontistis, Z.; Koutsoukos, P. G.; Vayenas, D. V. Pilot-Scale Hybrid System Combining Hydrodynamic Cavitation and Sedimentation for the Decolorization of Industrial Inks and Printing Ink Wastewater. *J. Environ. Manage.* **2022**, *302*, 114108.

(7) Robinson, T.; McMullan, G.; Marchant, R.; Nigam, P. Remediation of Dyes in Textile Effluent: A Critical Review on Current Treatment Technologies with a Proposed Alternative. *Bioresour. Technol.* **2001**, *77*, 247−255.

(8) Paz, A.; Carballo, J.; Pérez, M. J.; Domínguez, J. M. Biological Treatment of Model Dyes and Textile Wastewaters. *Chemosphere* **2017**, *181*, 168−177.

(9) Rauf, M. A.; Salman Ashraf, S. Survey of Recent Trends in Biochemically Assisted Degradation of Dyes. *Chem. Eng. J.* **2012**, *209*, 520−530.
(10) Pan, Y.; Wang, Y.; Zhou, A.; Wang, A.; Wu, Z.; Lv, L.; Li, X.; Zhang, K.; Zhu, T. Removal of Azo Dye in an Up-Flow Membrane-Less Bioelectrochemical System Integrated with Bio-Contact Oxidation Reactor. *Chem. Eng. J.* **2017**, *326*, 454−461.
(11) Chauhan, P. S.; Kant, R.; Rai, A.; Gupta, A.; Bhattacharya, S. Facile Synthesis of ZnO/GO Nanoflowers over Si Substrate for Improved Photocatalytic Decolorization of MB Dye and Industrial Wastewater under Solar Irradiation. *Mater. Sci. Semicond. Process.* **2019**, *89*, 6−17.
(12) Osagie, C.; Othmani, A.; Ghosh, S.; Malloum, A.; Kashitarash Esfahani, Z.; Ahmadi, S. Dyes Adsorption from Aqueous Media through the Nanotechnology: A Review. *J. Mater. Res. Technol.* **2021**, *14*, 2195−2218.
(13) Liu, L.; Chen, Z.; Zhang, J.; Shan, D.; Wu, Y.; Bai, L.; Wang, B. Treatment of Industrial Dye Wastewater and Pharmaceutical Residue Wastewater by Advanced Oxidation Processes and Its Combination with Nanocatalysts: A Review. *J. Water Process Eng.* **2021**, *42*, 102122.
(14) Boczkaj, G.; Fernandes, A. Wastewater Treatment by Means of Advanced Oxidation Processes at Basic PH Conditions: A Review. *Chem. Eng. J.* **2017**, *320*, 608−633.
(15) Moeen, S.; Ikram, M.; Haider, A.; Haider, J.; Ul-Hamid, A.; Nabgan, W.; Shujah, T.; Naz, M.; Shahzadi, I. Comparative Study of Sonophotocatalytic, Photocatalytic, and Catalytic Activities of Magnesium and Chitosan-Doped Tin Oxide Quantum Dots. *ACS Omega* **2022**, *7*, 46428−46439.
(16) Basu, A. K.; Chauhan, P. S.; Awasthi, M.; Bhattacharya, S. α-Fe2O3 loaded rGO nanosheets based fast response/recovery CO gas sensor at room temperature. *Appl. Surf. Sci.* **2019**, *465*, 56−66.
(17) Chauhan, P. S.; Kumar, K.; Singh, K.; Bhattacharya, S. Fast Decolorization of Rhodamine-B Dye Using Novel V2O5-RGO Photocatalyst under Solar Irradiation. *Synth. Met.* **2022**, *283*, 116981.
(18) Chauhan, P. S.; Kumar, S.; Mondal, A.; Sharma, P.; Parekh, M. N.; Panwar, V.; Rao, A. M.; Misra, A. Stacked Vanadium Pentoxide-Zinc Oxide Interface for Optically-Chargeable Supercapacitors †. *J. Mater. Chem. A* **2022**, *11*, 95.
(19) Gupta, A.; Saurav, J. R.; Bhattacharya, S. Solar Light Based Degradation of Organic Pollutants Using ZnO Nanobrushes for Water Filtration. *RSC Adv.* **2015**, *5*, 71472−71481.
(20) Gupta, A.; Bhattacharya, S. On the Growth Mechanism of ZnO Nano Structure via Aqueous Chemical Synthesis. *Appl. Nanosci.* **2018**, *8*, 499−509.
(21) Grilla, E.; Matthaiou, V.; Frontistis, Z.; Oller, I.; Polo, I.; Malato, S.; Mantzavinos, D. Degradation of Antibiotic Trimethoprim by the Combined Action of Sunlight, TiO2 and Persulfate: A Pilot Plant Study. *Catal. Today* **2019**, *328*, 216−222.
(22) Frontistis, Z.; Antonopoulou, M.; Venieri, D.; Dailianis, S.; Konstantinou, I.; Mantzavinos, D. Solar Photocatalytic Decomposition of Ethyl Paraben in Zinc Oxide Suspensions. *Catal. Today* **2017**, *280*, 139−148.
(23) Wang, D.; Mukhtar, A.; Humayun, M.; Wu, K.; Du, Z.; Wang, S.; Zhang, Y. A Critical Review on Nanowire-Motors: Design, Mechanism and Applications. *Chem. Rec.* **2022**, *22*, No. e202200016.
(24) Wang, D.-S.; Mukhtar, A.; Wu, K.-M.; Gu, L.; Cao, X. Multi-Segmented Nanowires: A High Tech Bright Future. *Materials* **2019**, *12*, 3908.
(25) Biswal, H. J.; Yadav, A.; Vundavilli, P. R.; Gupta, A. High Aspect ZnO Nanorod Growth over Electrodeposited Tubes for Photocatalytic Degradation of EtBr Dye. *RSC Adv.* **2021**, *11*, 1623−1634.
(26) Ameen, F.; Dawoud, T.; AlNadhari, S. Ecofriendly and Low-Cost Synthesis of ZnO Nanoparticles from Acremonium Potronii for the Photocatalytic Degradation of Azo Dyes. *Environ. Res.* **2021**, *202*, 111700.
(27) Weidner, E.; Karbassiyazdi, E.; Altaee, A.; Jesionowski, T.; Ciesielczyk, F. Hybrid Metal Oxide/Biochar Materials for Wastewater Treatment Technology: A Review. *ACS Omega* **2022**, *7*, 27062−27078.
(28) Bekris, L.; Frontistis, Z.; Trakakis, G.; Sygellou, L.; Galiotis, C.; Mantzavinos, D. Graphene: A New Activator of Sodium Persulfate for the Advanced Oxidation of Parabens in Water. *Water Res.* **2017**, *126*, 111−121.
(29) Maruthapandi, M.; Kumar, V. B.; Luong, J. H. T.; Gedanken, A. Kinetics, Isotherm, and Thermodynamic Studies of Methylene Blue Adsorption on Polyaniline and Polypyrrole Macro−Nanoparticles Synthesized by C-Dot-Initiated Polymerization. *ACS Omega* **2018**, *3*, 7196−7203.
(30) Mahdavi, R.; Ashraf Talesh, S. S. Enhanced Selective Photocatalytic and Sonocatalytic Degradation in Mixed Dye Aqueous Solution by ZnO/GO Nanocomposites: Response Surface Methodology. *Mater. Chem. Phys.* **2021**, *267*, 124581.
(31) Zhang, W.; Xu, H.; Xie, F.; Ma, X.; Niu, B.; Chen, M.; Zhang, H.; Zhang, Y.; Long, D. General Synthesis of Ultrafine Metal Oxide/Reduced Graphene Oxide Nanocomposites for Ultrahigh-Flux Nanofiltration Membrane. *Nat. Commun.* **2022**, *13*, 471.
(32) Gupta, A.; Mondal, K.; Sharma, A.; Bhattacharya, S. Superhydrophobic Polymethylsilsesquioxane Pinned One Dimensional ZnO Nanostructures for Water Remediation through Photocatalysis. *RSC Adv.* **2015**, *5*, 45897−45907.
(33) Chauhan, P. S.; Kant, R.; Rai, A.; Gupta, A.; Bhattacharya, S. Facile Synthesis of ZnO/GO Nanoflowers over Si Substrate for Improved Photocatalytic Decolorization of MB Dye and Industrial Wastewater under Solar Irradiation. *Mater. Sci. Semicond. Process.* **2019**, *89*, 6−17.
(34) Monteagudo, J. M.; Durán, A.; Martín, I. S.; García, S. Ultrasound-Assisted Homogeneous Photocatalytic Degradation of Reactive Blue 4 in Aqueous Solution. *Appl. Catal., B* **2014**, *152*−*153*, 59−67.
(35) Baxter, J. B.; Aydil, E. S. Nanowire-Based Dye-Sensitized Solar Cells. *Appl. Phys. Lett.* **2005**, *86*, 053114.
(36) Yang, K.; Feng, L.; Hong, H.; Cai, W.; Liu, Z. Preparation and Functionalization of Graphene Nanocomposites for Biomedical Applications. *Nat. Protoc.* **2013**, *8*, 2392−2403.
(37) Zhang, W.; Xu, H.; Xie, F.; Ma, X.; Niu, B.; Chen, M.; Zhang, H.; Zhang, Y.; Long, D. General Synthesis of Ultrafine Metal Oxide/Reduced Graphene Oxide Nanocomposites for Ultrahigh-Flux Nanofiltration Membrane. *Nat. Commun.* **2022**, *13*, 471.
(38) Vayssieres, L. Growth of Arrayed Nanorods and Nanowires of ZnO from Aqueous Solutions. *Adv. Mater.* **2003**, *15*, 464−466.
(39) Galvanin, F.; Al-Rifai, N.; Cao, E.; Sankar, M.; Hutchings, G.; Gavriilidis, A.; Dua, V. Merging Information from Batch and Continuous Flow Experiments for the Identification of Kinetic Models of Benzyl Alcohol Oxidation over Au-Pd Catalyst. In *26th European Symposium on Computer Aided Process Engineering*; Kravanja, Z., Bogataj, M., Eds.; Computer Aided Chemical Engineering; Elsevier, 2016; Vol. *38*, pp 961−966.
(40) Emady, H. N.; Wittman, M.; Koynov, S.; Borghard, W. G.; Muzzio, F. J.; Glasser, B. J.; Cuitino, A. M. A Simple Color Concentration Measurement Technique for Powders. *Powder Technol.* **2015**, *286*, 392−400.
(41) Saranya, M.; Ramachandran, R.; Wang, F. Graphene-Zinc Oxide (G-ZnO) Nanocomposite for Electrochemical Supercapacitor Applications. *J. Sci.: Adv. Mater. Devices* **2016**, *1*, 454−460.
(42) Sundriyal, P.; Bhattacharya, S. Inkjet-Printed Electrodes on A4 Paper Substrates for Low-Cost, Disposable, and Flexible Asymmetric Supercapacitors. *ACS Appl. Mater. Interfaces* **2017**, *9*, 38507−38521.
(43) Sundriyal, P.; Bhattacharya, S. Textile-Based Supercapacitors for Flexible and Wearable Electronic Applications. *Sci. Rep.* **2020**, *10*, 13259.
(44) Sajid, M. M.; Khan, S. B.; Shad, N. A.; Amin, N.; Zhang, Z. Visible Light Assisted Photocatalytic Degradation of Crystal Violet Dye and Electrochemical Detection of Ascorbic Acid Using a BiVO 4 /FeVO 4 Heterojunction Composite. *RSC Adv.* **2018**, *8*, 23489−23498.

https://doi.org/10.1021/acsomega.3c03122
ACS Omega 2023, 8, 28615−28627

(45) Akande, T.; Khatib, M.; Ola Salawu, S.; Afolabi Akindahunsi, A.; Di Cesare Mannelli, L.; Ghelardini, C.; Balli, D.; Cecchi, L.; Mulinacci, N. 1H NMR and HPLC-DAD-MS for the Characterization of Ellagitannins and Triterpenoids of Less Investigated Anogeissus Leiocarpus DC (Combretaceae) Stem Bark. *Food Chem.* **2022**, *375*, 131813.
(46) Qiu, Y.; Ma, C. HPLC, Quantitative NMR and HRMS Spectroscopic Data of Nusbiarylins as a New Class of Antimicrobial Agents. *Data Brief* **2020**, *29*, 105313.
(47) Liu, Y.; Sui, X.; Terán, J. E.; Chapman, L. P.; Ankeny, M.; Vinueza, N. R. Separation and Identification of Commercial Reactive Dyes with Hydrophilic Interaction Liquid Chromatography and Quadrupole Time-of-flight Mass Spectrometry. *Color. Technol.* **2021**, *137*, 407−417.
(48) Meetani, M. A.; Rauf, M. A.; Hisaindee, S.; Khaleel, A.; AlZamly, A.; Ahmad, A. Mechanistic Studies of Photoinduced Degradation of Orange G Using LC/MS. *RSC Adv.* **2011**, *1*, 490.
(49) Hisaindee, S.; Meetani, M. A.; Rauf, M. A. Application of LC-MS to the Analysis of Advanced Oxidation Process (AOP) Degradation of Dye Products and Reaction Mechanisms. *TrAC, Trends Anal. Chem.* **2013**, *49*, 31−44.
(50) Yang, K.; Feng, L.; Hong, H.; Cai, W.; Liu, Z. Preparation and Functionalization of Graphene Nanocomposites for Biomedical Applications. *Nat. Protoc.* **2013**, *8*, 2392−2403.
(51) Chauhan, P. S.; Kant, R.; Rai, A.; Gupta, A.; Bhattacharya, S. Facile Synthesis of ZnO/GO Nanoflowers over Si Substrate for Improved Photocatalytic Decolorization of MB Dye and Industrial Wastewater under Solar Irradiation. *Mater. Sci. Semicond. Process.* **2019**, *89*, 6−17.
(52) Wu, D.; An, T.; Li, G.; Wang, W.; Cai, Y.; Yip, H. Y.; Zhao, H.; Wong, P. K. Mechanistic Study of the Visible-Light-Driven Photocatalytic Inactivation of Bacteria by Graphene Oxide-Zinc Oxide Composite. *Appl. Surf. Sci.* **2015**, *358*, 137−145.
(53) Konwer, S.; Guha, A. K.; Dolui, S. K. Graphene Oxide-Filled Conducting Polyaniline Composites as Methanol-Sensing Materials. *J. Mater. Sci.* **2012**, *48*, 1729−1739.
(54) Chen, N.; Li, X.; Wang, X.; Yu, J.; Wang, J.; Tang, Z.; Akbar, S. A. Enhanced Room Temperature Sensing of Co3O4- Intercalated Reduced Graphene Oxide Based Gas Sensors. *Sens. Actuators, B* **2013**, *188*, 902−908.
(55) Shabir, M.; Yasin, M.; Hussain, M.; Shafiq, I.; Akhter, P.; Nizami, A.-S.; Jeon, B.-H.; Park, Y.-K. A Review on Recent Advances in the Treatment of Dye-Polluted Wastewater. *J. Ind. Eng. Chem.* **2022**, *112*, 1−19.
(56) Más-Montoya, M.; Janssen, R. A. J. The Effect of H- and J-Aggregation on the Photophysical and Photovoltaic Properties of Small Thiophene-Pyridine-DPP Molecules for Bulk-Heterojunction Solar Cells. *Adv. Funct. Mater.* **2017**, *27*, 1605779.
(57) Sterenzon, E.; Vadivel, V. K.; Gerchman, Y.; Luxbacher, T.; Narayanan, R.; Mamane, H. Effective Removal of Acid Dye in Synthetic and Silk Dyeing Effluent: Isotherm and Kinetic Studies. *ACS Omega* **2022**, *7*, 118−128.
(58) Sachin; Pramanik, B. K.; Gupta, H.; Kumar, S.; Tawale, J. S.; Shah, K.; Varathan, E.; Singh, N. Development of a ZnOS+C Composite as a Potential Adsorbent for the Effective Removal of Fast Green Dye from Real Wastewater. *ACS Omega* **2023**, *8*, 9230−9238.
(59) Wu, Z.; Wang, H.; Xue, Y.; Li, B.; Geng, B. ZnO Nanorods/ZnSe Heteronanostructure Arrays with a Tunable Microstructure of ZnSe Shell for Visible Light Photocatalysis. *J. Mater. Chem. A* **2014**, *2*, 17502−17510.
(60) Li, B.; Cao, H. ZnO@graphene Composite with Enhanced Performance for the Removal of Dye from Water. *J. Mater. Chem.* **2011**, *21*, 3346−3349.
(61) Holčapek, M.; Jandera, P.; Přikryl, J. Analysis of Sulphonated Dyes and Intermediates by Electrospray Mass Spectrometry. *Dyes Pigm.* **1999**, *43*, 127−137.
(62) Miranda-García, N.; Suárez, S.; Maldonado, M. I.; Malato, S.; Sánchez, B. Regeneration Approaches for TiO2 Immobilized Photocatalyst Used in the Elimination of Emerging Contaminants in Water. *Catal. Today* **2014**, *230*, 27−34.
(63) Chauhan, P. S.; Kant, R.; Rai, A.; Gupta, A.; Bhattacharya, S. Facile Synthesis of ZnO/GO Nanoflowers over Si Substrate for Improved Photocatalytic Decolorization of MB Dye and Industrial Wastewater under Solar Irradiation. *Mater. Sci. Semicond. Process.* **2019**, *89*, 6−17.

https://doi.org/10.1021/acsomega.3c03122
ACS Omega 2023, 8, 28615−28627